ACS Catalysis

Perspective

pubs.acs.org/acscatalysis

Identifying "Optimal" Electrocatalysts: Impact of Operating Potential and Charge Transfer Model

Alex M. Román,[†,‡] Jessica Dudoff,[‡,§] Adam Baz,[†,‡] and Adam Holewinski*[,†,‡,§]

[†]Department of Chemical and Biological Engineering, [‡]Renewable and Sustainable Energy Institute, and [§]Materials Science and Engineering Program, University of Colorado, Boulder, Colorado 80309, United States

ABSTRACT: Understanding the influence of potential on electrochemical surface reaction kinetics remains a challenge in identifying catalytic materials for numerous important reactions including water splitting (OER), hydrogen evolution (HER), and CO_2 reduction, among others. Limitations in computational methods, complicated by the unique environment of the electrode−electrolyte interface, have compelled many studies to focus on the thermodynamics of reaction schemes and to generalize inferences about the kinetics of charge transfer. In instances where activation barrier estimates are available, they are typically assumed to follow the empirical Butler−Volmer (BV) model. In this Perspective, we illustrate that the relative magnitudes and potential-dependences of elementary barriers can have a marked effect on the properties of a catalyst deemed "optimal" for a given reaction. We use a simple pseudosteady-state analysis of two sequential surface-mediated charge transfers to assess the degree of rate control of each step as a function of the material and conditions. We compare BV kinetics to Marcus theory and also discuss more recent models that are specific to the interactions of an adsorbate with the electronic structure of a surface. Recent developments in the full simulation of charge transfer to surface species are also briefly discussed. Finally, we highlight the need for assessment of kinetics and identification of activity descriptors that are optimal *at relevant operating conditions,* and we conclude with an outlook on current research needs.

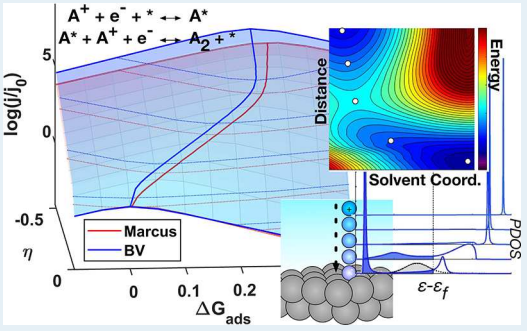

KEYWORDS: *electrocatalysis, electron transfer, microkinetic modeling, Marcus theory, symmetry factor, hydrogen evolution*

INTRODUCTION

Electrocatalytic reactions are at the forefront of contemporary research due to their promising role in sustainable energy conversion.[1−3] However, it remains a challenge to optimize catalytic materials to navigate the complex energy landscapes that govern most transformations of interest, both in electrocatalysis and in heterogeneous catalysis in general. The electrochemical environment poses unique difficulties, with solvent, electrolyte ions, electrode potential, and the interfacial field all playing roles that can be difficult to quantify.[4] These complexities beget a corresponding knowledge gap in comparison to thermally driven reactions; in particular, the dynamical processes involved in electrochemical activation are notoriously difficult to interrogate.

Significant progress has been made in recent years toward the explicit evaluation of activation barriers for elementary electrochemical surface processes—most notably through the use of quantum chemical calculations.[5−7] Nonetheless, the computational costs and uncertainties associated with these methods have driven a majority of studies to base analyses of electrocatalytic activity on the pure thermodynamics of proposed elementary steps. Specifically, it is common practice to identify catalytic material candidates with the criterion that they minimize the overpotential needed to make all elementary steps either energetically neutral or downhill.[8] In most instances where microkinetic models have been built from barrier estimates,[9−12] the treatment has been restricted to the phenomenological Butler−Volmer (BV) framework, which assumes that activation barriers shift linearly with respect to potential. While more encompassing theories of electron transfer predict deviations from BV kinetics, the extent to which these deviations may be significant (with respect to identifying optimal electrocatalysts) is generally assumed negligible and rarely discussed.

In this contribution, we examine the criteria for identifying an "optimal" catalyst for a simple two-step mechanism involving an adsorbed intermediate. In this context, an "optimal" material will be defined as one that possesses a value for an activity descriptor (e.g., the binding energy of a key intermediate) that maximizes the predicted rate *within a given kinetic model*. For clarity, we also differentiate kinetic models—which permit extrapolation of explicitly calculated or measured barriers—from the interfacial models and referencing schemes involved in such explicit evaluations. We compare rates determined by BV kinetics to Marcus theory, and then discuss more recent approaches to modeling the interactions between a redox species and the electronic structure of an electrode surface. Our analysis indicates that model choice may be

Received: September 21, 2017
Revised: November 13, 2017
Published: November 15, 2017

DOI: 10.1021/acscatal.7b03235
ACS Catal. 2017, 7, 8641−8652

secondary in importance to obtaining accurate barrier values, but that the model can still be critical if calculated barriers must be extrapolated over significant potential ranges. Most importantly, we highlight that the best material choice depends on operating potential.

It is worth mentioning that a variation in optimal catalyst material with operating conditions is well-established in heterogeneous catalysis. For example, the water−gas-shift reaction is typically carried out in two catalytic stages—a high temperature stage for high initial rates followed by a lower temperature stage permitting greater equilibrium conversion—each over catalysts that work best at the given conditions.[13] Similarly, ammonia synthesis has been shown to be most efficient over staged or gradient catalyst beds, with a varying formulation optimized for specific concentrations.[14,15] Such principles have yet to find use in electrochemical processes, and a critical step toward better-informed catalyst choice will be the establishment of sufficiently accurate models for the potential-dependence of the kinetics. In writing a Perspective, our goal is not to provide a comprehensive review of approaches to modeling electrocatalytic reactions, but rather to highlight the implications of using approaches with varying degrees of detail to optimize a given activity descriptor. We thus hope to underscore the importance of balancing tractability with rigor in kinetic frameworks.

ACTIVITY DESCRIPTORS AND THE TRANSFER COEFFICIENT AS A BEP RELATION

For the sake of discussion, we consider the following two-step reaction scheme:

$$A^+ + e^- + * \leftrightarrow A^* \quad \text{(R1)}$$

$$A^* + A^+ + e^- \leftrightarrow A_2 + * \quad \text{(R2a)}$$

$$2A^* \leftrightarrow A_2 + 2^* \quad \text{(R2b)}$$

The above scheme could represent the hydrogen evolution reaction (HER), although we intend to keep the discussion more general. One notable feature of the reaction scheme is that the product (A_2) may form by either electrochemical (R2a) or pure chemical (R2b) pathways. Naturally, the rate of the former can be expected to exhibit much stronger sensitivity to potential, and the dominant pathway may thus depend on operating conditions. However, even in a case where a pure electrochemical pathway is followed (e.g., steps R1 and R2a only), it is not necessarily true that each step in the sequence will respond in the same manner to potential or that a given step will retain rate control at all potentials. Additionally, cases may arise where the step identified as "rate-determining" (RDS) differs from the most endergonic, or "potential-determining" step (PDS).[16] To focus on the underlying phenomena, we will restrict analysis to the pure electrochemical case.

Rough guidance toward the optimization of catalytic activity can be found in the form of the Sabatier principle,[17] which stipulates that catalytic materials should bind surface intermediates neither too strongly nor too weakly, lest the reaction be limited by either removal of products or activation of reactants. This trade-off implies that there exists an optimal degree of surface reactivity, prompting the well-known concept of a volcano relationship. The affinity of a surface for intermediates is generally quantified by the adsorption energy of a key representative species, and correlating the activity with such a descriptor often captures broad trends well.[18−20] The successes of this approach can be understood in terms of the Brønsted−Evans−Polanyi (BEP) principle of free energy scaling,[21,22] which dictates that activation barriers should shift (linearly) in proportion to the reaction energy. A schematic free energy diagram illustrating the effect of changing ΔG_{ads} for the reaction scheme above is given in Figure 1b.

In a similar vein, adjusting the potential of an electrode changes the free energy of each electron transfer, with a corresponding shift in each activation barrier. Empirically, the dependence of the activation barrier on potential can be described by the transfer coefficient, α:

$$\alpha = -\frac{RT}{F}\frac{\partial \ln k}{\partial E} = \frac{1}{F}\frac{\partial \Delta G^{\ddagger}_{app}}{\partial E} \quad (1)$$

where k is the rate constant, $\Delta G^{\ddagger}_{app}$ is the apparent barrier, E is the potential, and the physical constants have their usual meaning. We will distinguish the apparent transfer coefficient for a multistep reaction, α, from that of elementary steps by using the alternative designation "symmetry factor," β, which applies specifically to the elementary case—i.e. the elementary transfer coefficient is the symmetry factor.[23] This parameter indicates that when a reaction energy shifts by a given amount, the activation barrier will undergo a fractional change of β. Thus, a constant symmetry factor may be interpreted as a manifestation of the BEP relation. It may be noted here that an overpotential corresponds to an efficiency loss, and is thus usually not a preferred lever to "tune" activity. Nonetheless there is a parallel to be drawn with changing adsorption energy. As illustrated in Figure 1a, the key difference is that an applied overpotential has the effect of shifting all electrochemical steps in the exergonic direction, rather than accelerating some at the expense of others. Throughout this discussion we adopt the sign convention that a negative overpotential increases the rate of reduction, as negative potentials increase electron energy.

In a BV model, symmetry factors are treated as constants, and it is common to assume that $\beta \approx 1/2$ for all elementary steps.[24,25] While $\beta \approx 1/2$ is a serviceable approximation, microscopic theories of charge transfer indicate that symmetry factors should vary continuously with potential. The dependence on potential can, in some instances, be weak; nonetheless, differences in elementary symmetry factors will alter the relative importance of each step as potential varies. An extreme example would be the electrochemical-chemical or "EC" pathway R1 + R2b, where the chemical step would show $\beta \approx 0$ (perhaps a weak dependence on field, concentration terms, etc.) and become increasingly rate-determining as potential is applied to accelerate the electrochemical step. For less dramatic differ-

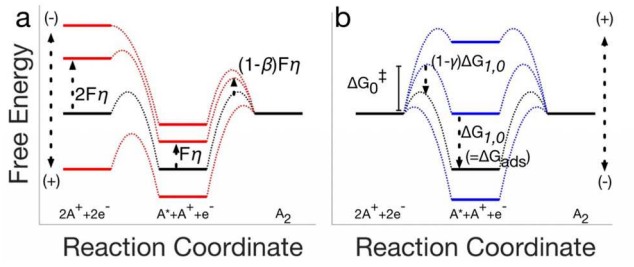

Figure 1. Schematic free energy diagrams for a two-step, two-electron transfer reaction with linear barrier scaling. (a) Varying overpotential. (b) Varying adsorption energy of the surface intermediate.

DOI: 10.1021/acscatal.7b03235
ACS Catal. 2017, 7, 8641−8652

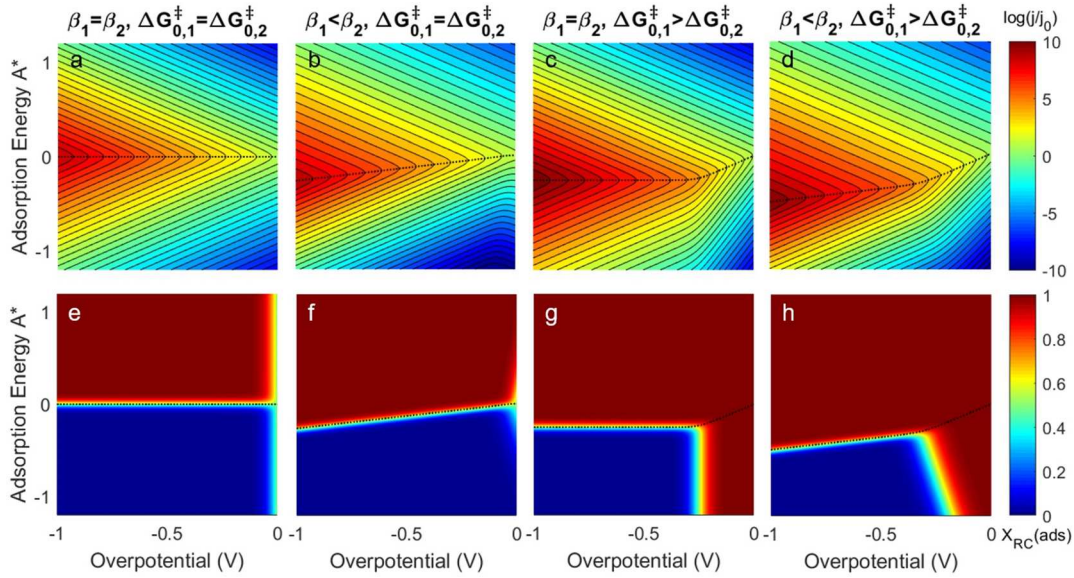

Figure 2. Activity maps (a–d) using BV model for two step electrochemical reaction scheme. In all cases $\gamma_i = \beta_i$. (a) Identical parameters: $\beta_1 = \beta_2 = 0.5$ and $\Delta G^{\ddagger}_{0,1} = \Delta G^{\ddagger}_{0,2} = 1$ eV. (b) Unequal symmetry factors: $\beta_1 = 0.3$, $\beta_2 = 0.7$, $\Delta G^{\ddagger}_{0,1} = \Delta G^{\ddagger}_{0,2} = 1$ eV. (c) Unequal intrinsic barriers: $\beta_1 = \beta_2 = 0.5$, $\Delta G^{\ddagger}_{0,1} = 1$, $\Delta G^{\ddagger}_{0,2} = 0.75$ eV. (d) Unequal symmetry factors and intrinsic barriers: $\beta_1 = 0.3$, $\beta_2 = 0.7$, $\Delta G^{\ddagger}_{0,1} = 1$, $\Delta G^{\ddagger}_{0,2} = 0.75$ eV. The black dotted lines denote the maximum rate at each potential. DRC plots (e–h) for reaction step R1 correspond to the activity maps directly above (a–d). All values are normalized to activity at 0 V with 0 eV adsorption energy.

ences in symmetry factors, the implication is still that the best catalyst identified for a particular potential may not be ideal for realistic or practical overpotentials—we will show below that even identical symmetry factors do not guarantee the optimal catalyst is independent of potential.

Considering each contribution to the activation barrier explicitly, a rate constant for a given step may be written as

$$k_i = A_{0,i}\exp[-(\Delta G^{\ddagger}_{0,i} + \beta_i F\eta + \gamma_i \Delta G_{0,i})/RT] \quad (2)$$

where η is the overall-reaction overpotential ($E - E^0$), γ_i is the (thermochemical) BEP coefficient, $\Delta G_{0,i}$ is the elementary reaction energy at zero overall-reaction overpotential ($\pm\Delta G_{ads}$ of 1/2 A_2 for each step here), $A_{0,i}$ is the pre-exponential factor, and $\Delta G^{\ddagger}_{0,i}$ is an "intrinsic" barrier, defined when the individual step is at equilibrium on a reference material exhibiting $\Delta G_{0,i} = 0$. The elementary reaction energy ($\Delta G_{0,i}$) may thus be more appropriately labeled a "ΔΔG" relative to the reference material, but the distinction is arbitrary for a reference of zero. Additionally, the intrinsic barrier ($\Delta G^{\ddagger}_{0,i}$) will be independent of the reference if $\beta = \gamma$. Because a strict BEP relation does not parse free energy change into chemical and electrochemical contributions, it may often be approximated that $\beta \approx \gamma$, though this is not inherently required—the factors embed potential-dependent and material-dependent properties, respectively. Given the analogy between each coefficient, β and γ will be referred to as the electrochemical symmetry factor (ESF) and thermochemical symmetry factor (TSF). We restrict the present analysis to the case in which both quantities are equal. Equation 2 is equivalent to the Butler-Volmer model of electrode kinetics—that is, free energy curves for reactant and product (vs reaction coordinate, see Figure 3) are linear near the transition state. Consequently, changing a reactant energy (electrode potential) by a given amount ($F\eta$) moves the transition-state energy by a corresponding fractional amount ($[1 - \beta]F\eta$), with net barrier decrease $\beta F\eta$. The reverse of any given step thus also obeys $\beta_{-i} = (1 - \beta_i)$. Deviations from $\beta = 1/2$ can be interpreted as a measure of the earliness or lateness of the transition state,[24] and measured values for single-electron transfer reactions usually range from ~0.3 to ~0.7 under typical experimentally accessible conditions.[26]

To a first approximation, it may be estimated that both reaction steps in consideration, R1 + R2a, will have $\beta_1 \approx \beta_2 \approx 0.5$ (and $\gamma_1 \approx \gamma_2 \approx 0.5$). Whenever $\beta_1 = \beta_2$, the ratio k_1:k_2 is independent of the overpotential. If both steps are irreversible, this leads to a total independence of the optimal adsorption energy with respect to potential. On the other hand, a simple steady-state analysis also stipulates that when all forward and reverse steps are considered, any difference in intrinsic barriers ($\Delta G^{\ddagger}_{0,i}$) will cause the optimal adsorption energy to vary from zero near equilibrium to a new constant at large overpotential. The impact of reversible elementary steps is an aspect of microkinetics that is perhaps even more important in electrocatalysis than in thermal processes—electrochemical half-reactions are ideally run very close to their individual equilibria, even though the overall cell reaction is far from equilibrium. The steady-state analysis when all steps are reversible is shown in Figure 2, and the specific case in which intrinsic barriers differ is shown in Figure 2c. There, the variation in optimal adsorption energy may be understood from the perspective that when $\eta = 0$, a value of $\Delta G_{ads} = 0$ balances the net rates of adsorption and desorption. The maximum activity (dotted lines in Figure 2) coincides with an adsorbate coverage of 1/2, which is established if each elementary step is near equilibrium, regardless of their individual intrinsic barriers. As overpotential increases, reverse rates become negligible, and the optimal ΔG_{ads} is the one that causes the apparent barriers of each step to equalize—for the scenario where all symmetry factors are 1/2 this happens to occur when ΔG_{ads} is equal to the difference in intrinsic barriers. Hence, a difference of say 0.25 eV in $\Delta G^{\ddagger}_0$ values would be expected to cause a 0.25 eV shift in optimal adsorption energy with potential, as shown in Figure 2c. Differences between ESFs ($\beta_1 \neq \beta_2$), further influence the

DOI: 10.1021/acscatal.7b03235
ACS Catal. 2017, 7, 8641–8652

relative importance of each step such that there is no asymptotic limit to the optimal value (Figure 2b,d).

Examining the degree of rate control (DRC) for each step ($X_{RC,i} = [\partial \ln r/\partial \ln k_i]_{k_{j\neq i},K_i}$[27,28] as a function of potential provides further insight into the limiting processes. The DRC is essentially a sensitivity analysis with respect to each transition-state energy and is shown in Figure 2e−h for each scenario mapped in Figure 2a−d. In the case where all parameters are equal (Figure 2a), the maximum rate occurs when $\Delta G_{ads} = 0$, and each step exhibits equal control over the rate at all potentials. In the case of more exergonic adsorption energies, the rate falls but, notably, the DRC does not immediately change near the equilibrium potential (right side of Figure 2e). This is a consequence of the inclusion of reverse reactions and compensating influences between rate constants and available sites—raising ΔG_{ads} (relative to an exergonic value) better balances adsorptive and desorptive processes, but there is still not a single transition-state governing the rate. When overpotential is increased in conjunction with the use of an exergonic material, the product formation step and its associated transition state then emerge as completely rate controlling.

Moving to the case where symmetry factors differ (Figure 2b), a new behavior is exhibited whereby a trade-off in limiting step can be seen at large overpotential. This corresponds to the optimal value of adsorption energy continually decreasing, shifting the limiting step from R2a to R1 for materials in the range of mildly exergonic ΔG_{ads}. Finally, when the intrinsic barriers differ (Figure 2c,d), the rate-determining step is identified solely as the process with the higher intrinsic barrier unless both adsorption energy and overpotential are large. At smaller overpotentials, this scenario leads to a regime in which the optimum adsorption energy does not correspond to an equal DRC from each step. This is the case mentioned earlier in which the rate-determining step differs from the potential-determining step. The magnitude of the rate can be modulated by the barrier of the first step, while the second step barrier has no impact. Nonetheless, the second step is also critical as it dictates a thermodynamically controlled (i.e., quasi-equilibrated) active-site fraction.[29] Such a phenomenon has been discussed with respect to the kinetics of ORR on Pt, which shows a Tafel slope and other kinetic signatures that are indicative of limitation by activation, but which exhibits higher rates on materials that bind oxygen more weakly than Pt.[30,31] In such cases, it could in principle be possible to accelerate the rate by selectively lowering the initial O_2 activation barrier. Scaling relations may often prevent such a strategy in practice, but it is worth consideration.

The above analysis presumes that elementary barriers and symmetry factors are apt to show appreciable differences for various elementary steps. It is not immediately clear, however, that such regimes will appear in electrocatalytic processes of interest—many of these processes (e.g., ORR, OER, HOR, HER, CO_2 reduction) are believed to proceed through series of chemically similar proton-coupled electron transfer steps.[30,32−36] Thus, we next discuss some simple models of the electrochemical activation process in order to explore the extent to which such phenomena might be relevant.

MICROSCOPIC MODELS OF ELECTRON TRANSFER

Modern theories of charge transfer generally have origins attributable to the work of Marcus[37] and Hush.[38] Marcus originally proposed that solvent reorganization plays a major role in activation via fluctuations, which lead to a non-equilibrium polarization with respect to the electrostatic field of the reactants or products. While the electron cloud of solvent molecules can polarize quickly in response to charge transfer, the slow solvent modes involved in reorientation cannot. A reaction coordinate may thus be identified as a reorientation of solvent between a configuration that would be in equilibrium with the reactants and one corresponding to equilibrium with the products. The "outer" reactant energy associated with solvent reorganization is then given by the change (upon charge transfer) in total solvation energy, minus that due to the fast modes. Based on the approximation of solvent as a continuum dielectric, this is roughly

$$\lambda_O = \frac{(\Delta e)^2}{8\pi\varepsilon_0}\frac{1}{a_0}\left(\frac{1}{\varepsilon_\infty} - \frac{1}{\varepsilon_r}\right) \tag{3}$$

where Δe is the charge transferred, ε_∞ and ε_r are the optical and static dielectric constants, and a_0 is the radius of the reacting ion. Additional terms may be added to account for an image charge interaction on an electrode and/or cases of bimolecular reactions. If the reaction coordinate, q_s, represents the solvent orientation that would be in equilibrium with a given extent of charge transfer (i.e., $\Delta e = q_s e_0$) then the resulting free energy surface of both reactants and products can be considered parabolic.[39] Moreover, addition of any "inner" reorganization energy (λ_I) in the form of changes to normal harmonic vibrational modes will retain the parabolic nature of the free energy surfaces along the reaction coordinate. With appropriate coordinate scaling one can describe the reactant and product surfaces by one effective reaction coordinate (q) and the total reorganization energy $\lambda = \lambda_O + \lambda_I$, such that, for example, the reactant energy is simply λq^2.

A critical point for consideration in catalysis is that Marcus theory treats reaction rates only in the limit of weak electronic coupling between the wave functions of reacting species. The coupling is assumed to be sufficient for the transition to be adiabatic, but at the same time there is not a well-defined transition state. Electron transfer occurs when a nuclear configuration that could correspond to either product or reactant at the same energy is achieved, and the barrier is thus effectively located at the intersection of the free energy curves. As illustrated in Figure 3b, if the coupling element (V_{ab}) is small, the true location of the barrier may be reasonably estimated, but strong coupling introduces more uncertainty. A rigorous quantum treatment in the limit of very weak coupling was given originally by Levich and Dogonadze, addressing nonadiabaticity, tunneling, and (for heterogeneous cases) transfer to/from the continuum of states available on an electrode.[40,41] In contrast, the regime of strong coupling remains less well-described but is unfortunately the domain most relevant to electrocatalytic reactions. Strong coupling does generally permit the assumption of adiabaticity, but treatment of electron transfer to and from various electrode states must give way toward a treatment of hybridization and shared electrons between electrode and substrate.

Before discussing more contemporary approaches to electrode kinetics, we illustrate a few consequences of Marcus theory, as compared to the BV framework in Figure 3. Provided that vibrational force constants do not change substantially between reactants and products, both free energy parabolas will

DOI: 10.1021/acscatal.7b03235
ACS Catal. 2017, 7, 8641−8652

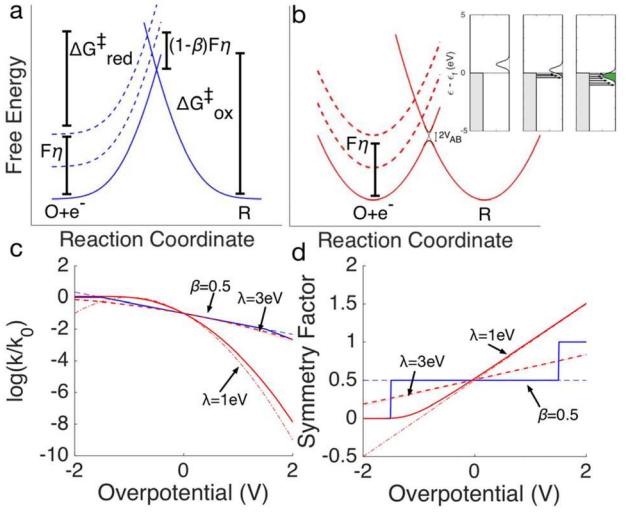

Figure 3. Representative free energy diagrams for (a) Butler–Volmer model and (b) Marcus theory electron transfers. "O" and "R" represent oxidized and reduced forms of a molecule. Inset: Band diagram of initial and final states for Gerischer–Marcus model, where rate is proportional to overlap. (c) Normalized rate constants and (d) corresponding symmetry factors as a function of overpotential for typical kinetic parameters, as labeled. For each curve marked by a λ value, the lighter weight line represents standard Marcus theory and the heavier line is the Gerischer modification. The BV barrier was set to 0.75 eV to coincide with the λ = 3eV Marcus model at equilibrium. Discontinuities in the solid BV curves represent a crossover to activationless and barrierless regimes, while the dotted lines show the result of eq 2 unrestricted.

have the same characteristic reorganization energy. The activation barrier is easily found at the intersection:

$$\Delta G_i^{\ddagger} = \frac{(\lambda_i + \Delta G_i)^2}{4\lambda_i} \tag{4}$$

For an electrode reaction in which the reactant can adsorb, we may express $\Delta G_i = \Delta G_{0,i} + F\eta$ (as defined for eq 2). At equilibrium, eq 4 yields a barrier of $\lambda_i/4$. The ESF may be determined from the derivative with respect to overpotential:

$$\beta_i = \frac{1}{2} + \frac{\Delta G_{0,i} + F\eta}{2\lambda_i} = \frac{1}{2} + \frac{F\eta_i}{2\lambda_i} \tag{5}$$

where we have noted the overpotential of an individual step to be $\eta_i = \Delta G_{0,i}/F + \eta$. It is also straightforward to show that the Marcus description requires a TSF $\gamma_i = \beta_i$. The relation in eq 5 implies that in an individual reaction, the symmetry factor spans the range of zero to unity over the course of an overpotential window of $\pm \lambda/F$, creating significant deviation from BV characteristics unless λ is large. Reorganization energies of outer-sphere electron transfer are typically on the order of 0.5–1 eV,[42] while estimates for the process of shedding a (partial) solvent layer to bond to an electrode can be significantly higher—a value of 3 eV has been suggested for reduction of an aqueous proton,[43] which is consistent with eq 3 using the solvation radius of H_3O^+ (~1 Å). The variation of rate constants with the values λ = 1 eV and λ = 3 eV is shown in Figure 3c. With values of the latter magnitude, deviation from a constant symmetry factor may be slow, but in a sequential mechanism, elementary steps may also require a large overpotential to become favorable. A highly unfavorable step would be expected to show an ESF near unity when the overall reaction is at equilibrium, while the ESF would shift nearer to 1/2 at the overpotentials where this step becomes downhill. Extreme overpotentials (>1 V) are commonly utilized in reactions such as oxygen evolution (OER) and the electroreduction of CO_2.[44,45]

It may be noted that in the limit of very large driving force, eqs 4 and 5 should yield an increasing barrier and negative symmetry factor. Such behavior is known as the "inverted regime" and can be seen in Figure 3 as a decreasing rate constant at large negative overpotential. Marcus theory approximates that the majority of electron transfer should occur to/from states near the Fermi level set by electrode potential, as these represent the largest driving force among appropriately populated states (e.g., highest energy states with electrons available for reduction). Unlike homogeneous electron transfers, however, the electrode may exchange electrons from any available level and should reach a current plateau rather than an inverted region. In a framework formulated by Gerischer,[46] the local rate (per unit energy level in the electrode) is considered proportional to the product of the electrode density of states (DOS) and the concentration of redox species (which exhibit a distribution of energies) that are aligned at the same level. For a simple metal electrode (treated as a reservoir of large, constant DOS), eq 4 can be used to infer a Gaussian distribution of local rates,[47] as illustrated in the inset of Figure 3b. Approximating the Fermi–Dirac distribution of electronic states, $f(\varepsilon)$, as a step function, one may write

$$k_i \propto \int \exp\left[-\frac{(\lambda_i + F\eta_i - \varepsilon')^2}{4RT\lambda_i}\right] f(\varepsilon')\mathrm{d}\varepsilon' \approx \mathrm{erfc}\left(\frac{\lambda_i + F\eta_i}{2\sqrt{RT\lambda_i}}\right) \tag{6}$$

where $\varepsilon' = \varepsilon - \varepsilon_f$. This yields

$$\beta_i = \sqrt{\frac{RT}{\pi\lambda_i}}\,\frac{\exp[-z^2]}{\mathrm{erfc}(z)} \tag{7}$$

where $z = \frac{\lambda_i + F\eta_i}{2\sqrt{RT\lambda_i}}$. Equations 6 and 7 yield asymptotic limits for the rate constant and ESF (zero) at large overpotential, and are compared to the BV and basic Marcus models in Figure 3. Deviations are seen to be minor with respect to Marcus theory, but they become significant for small reorganization energies and large exergonic overpotentials. While asymptotic behavior is not addressable by BV or simple Marcus kinetics, it is common practice in microkinetic modeling to impose cutoff points such that the barrier does not become negative (the "activationless" limit) or exceeded by reaction energy (the "barrierless" limit).[48]

Narrowing the focus to surface-mediated reactions, strong resonant coupling is to be expected between the reactant wave function and electrode band structure. While these interactions may be most accurately captured with numerical quantum chemical calculations, significant insight may be gained by examination of more approximate models. To this end it is helpful to define the energy of the complete reacting system, rather than producing separate reactant and product curves. Most important to this description, the energy level of the relevant orbital of the redox species has been shown, to good approximation, to couple with solvent modes in linear proportion to charge.[40] When the solvent coordinates are scaled by the linear coupling constants, the effective one-

DOI: 10.1021/acscatal.7b03235
ACS Catal. 2017, 7, 8641–8652

electron energy level (relative to that in vacuum) can then be described as

$$\tilde{\varepsilon}_{a,\sigma} = \varepsilon_{a,\sigma} - 2\lambda q + U\langle n_{a,-\sigma}\rangle \quad (8)$$

Equation 8 has the meaning that for occupation number $\langle n_{a,\sigma}\rangle$, the electronic energy of the state is $\langle n_{a,\sigma}\rangle\tilde{\varepsilon}_{a,\sigma}$ (where σ denotes spin). The solvent coupling term ($2\lambda q$) is defined here with the convention that a neutral species has occupation number $\langle n_{a,\sigma}\rangle = 0$ (equilibrium polarization at $q = 0$), and the final term represents on-site Coulomb repulsion of magnitude U. It has been suggested[49,50] to treat the hybridization of the effective redox level (eq 8) with electrode states according to the Newns–Anderson (NA) model of chemisorption.[51,52] Here we perform such an analysis for the reductive adsorption of H^+ on Pt using several ideas outlined in refs 49 and 50, but we have also made a few critical alterations. These works consider the electron transfer to involve a single spin state of the adsorbate, even when the spin states become degenerate at the short electrode-adsorbate separations relevant to adsorption. Our depiction effectively differs by accounting for both states so that the DOS projected onto the adsorbate orbital during adsorption still represents a capacity for two electrons.[53] Our development ultimately resembles more closely an effective-medium theory.[54] A more detailed description will be given elsewhere.

A simple formulation of the NA-model gives the (spin-unpolarized) adsorbate-localized DOS as

$$\rho_a(\varepsilon) = \frac{1}{\pi}\frac{\Delta(\varepsilon)}{[\varepsilon - \tilde{\varepsilon}_a - \Lambda(\varepsilon)]^2 + \Delta(\varepsilon)^2} \quad (9)$$

Above, the $\Delta(\varepsilon)$ term is a broadening proportional to the coupling matrix element (V_{a,M_k}) between the adsorbate level and each metal state, often treated as a constant (for fixed separation distance) such that $\Delta(\varepsilon)$ is proportional to the metal DOS: $\Delta(\varepsilon) = \pi V^2 \rho_M(\varepsilon)$. The $\Lambda(\varepsilon)$ term represents an energy shift, which in the limit of strong coupling to narrow bands (e.g., d-states) produces bonding and antibonding levels. It is given by the Hilbert transform of Δ:

$$\Lambda(\varepsilon) = \mathcal{P}\frac{1}{\pi}\int_{-\infty}^{\infty}\frac{\Delta(\varepsilon')}{\varepsilon - \varepsilon'}d\varepsilon' \quad (10)$$

In the limit of a flat band structure (e.g., *sp*-metals), $\Lambda \to 0$ and the broadening is simply Lorentzian. Representative plots for $\rho_a(\varepsilon)$ during the adsorption of H on a Pt surface, computed with DFT (VASP package[55,56]) and fit with eq 9 are shown in Figure 4.[53] We note that direct quantum chemical calculations are not necessary for a qualitative description, but extracting a few parameters from these calculations greatly simplifies discussion. Fits of $\rho_a(\varepsilon)$ were used to estimate the coupling matrix elements as well as the self-consistent vacuum adsorbate levels corresponding to each H-metal distance with the solvent coordinate $q = 0$ (reduced H atom). It should also be noted that despite any superficial resemblances, this adsorbate-localized DOS is fundamentally different than the distribution of available redox levels in Figure 3.

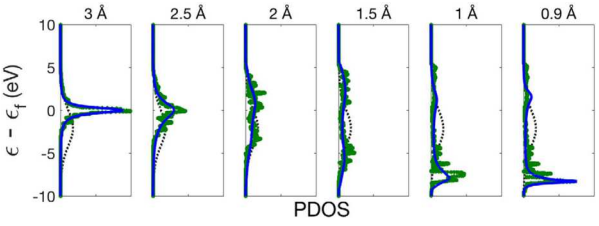

Figure 4. Calculated (green) and fit (blue) H_{1s} projected density of states[53] at various distances between H and the plane of a 3-fold hollow site of Pt(111). A Gaussian fit to the Pt d-band (dotted line) is also shown for reference. The sp-states were treated as a flat band in fits.

Equipped with the local DOS for the adsorbing species and a means to calculate its changes due to solvent fluctuation, the one electron energy sum (integration over the DOS) may be obtained. It has been well illustrated in the effective medium theory of Nørskov and co-workers[54,57] that changes to the one-electron sum upon adsorption will often capture differences in adsorption energies across a series of similar systems. This is a powerful result because the one-electron energy is not the only contribution to total energy. Briefly, in the effective medium theory, adsorption is governed mainly by the atom seeking a region of optimal electron density. When a system is perturbed by, for example, changing the chemical identity of the surface, the adsorbate will adjust its bond distance to re-establish a similar ambient electron density and thus experience a similar "embedding energy." *Differences* in adsorption energy are then governed by small corrections which amount to (i) the change in one-electron energy levels and (ii) changes in nonlocal electrostatic interactions. In this context, "nonlocal" refers to the interactions between the charge density in one region (e.g., the adsorbate) and the field emanating from the other region (e.g., the surface). The electrostatic contributions are often small, though they can play a significant role when strong dipoles or ions are present, as in alkali-promoted reactions[58,59] or, naturally, redox reactions.

In the present system, solvent fluctuations may be treated as a perturbation, modifying the H-metal interaction relative to the value in the absence of solvent at a given H-metal separation. With solvent terms, the change in adsorption energy (at fixed distance and zero overpotential) can then be estimated as

$$\Delta E(q) = \Delta E|_{q=0} + \delta E_{1e}(q) + \delta E_{es}(q) + \lambda q^2 + 2\lambda q \quad (11)$$

where:

$$\delta E_{1e} = \int_{-\infty}^{\varepsilon_f}[\tilde{\rho}_a(\varepsilon) - \rho_a(\varepsilon)]\cdot\varepsilon d\varepsilon$$

$$\delta E_{es} = \phi(1 - \langle n_a\rangle)$$

Above, Δ indicates the change upon adsorption while δ indicates a change upon perturbation by a solvent fluctuation. Perturbed quantities are denoted by a tilde. The first term in eq 11 is simply the adsorption energy in the absence of solvent. The electrostatic energy term represents the interaction of the field of the electrode (screened potential, ϕ, relative to the bulk solution, at distance d), with the charge of the adsorbate (proton). To higher order, a polarization term could also be added to account for the image charge induced in the electrode, but the electrostatic contribution was found to be small here and does not impact the discussion. The last term emanates from eq 8 by assigning the proton a coordinate of $q = -1$ and a charge of $1 - \langle n_a\rangle$, rather than $\langle n_a\rangle$. Finally, we can estimate the free energy (relative to $H^+ + e^-$ at 0 V_{RHE}), by adding the contributions of overpotential, entropy, and zero-point energy, each proportional to the charge transferred: $\Delta G = \Delta E(q) + e_0\eta(1 - \langle n_a\rangle) + (\Delta ZPE - T\Delta S)\langle n_a\rangle$. While the energy

DOI: 10.1021/acscatal.7b03235
ACS Catal. 2017, 7, 8641–8652

associated with overpotential should indeed shift linearly with the extent of charge transfer, the latter terms are effectively an interpolation between tabulated[60,61] initial and final values. The resulting free energy surface at $\eta = 0$ is presented in Figure 5a, along with corresponding DOS plots showing how the occupation of the H-orbital changes along the reaction coordinate (Figure 5c).

Before interpreting the free energy surface, it should be noted that the effective medium theory approximates that there is no change to exchange and correlation energies upon perturbation. Since the orbital occupancies in the present model change more dramatically than in the case of shifting across various transition metal surfaces, this approximation represents a weakness in our depiction. The allocation of charge to the adsorbate also raises an interesting issue. One may note that the occupation of the adsorbate state is estimated by $\langle n_a \rangle = \int_{-\infty}^{\epsilon_f} \rho_a(\epsilon) d\epsilon$, where proper normalization of ρ_a permits an occupancy up to two electrons. As the adsorbed H atom reaches its final bond length, the band occupancy tends to exceed 1 (i.e., the one electron introduced by charge transfer). More complex spatial-allocation schemes such as Bader analysis[62] give similar results. Thus, separating the contributions of charge transfer and local hybridization (i.e., bond polarity) from a simulation is nontrivial. One computational test that has been suggested is to compare the dependence of the adsorption energy on the work function of the surface (modified with remote coadsorbates).[10] This can help to diagnose the absence of true charge transfer, but if both phenomena are simultaneous, the interpretation is less clear. In some studies, hybridization has been considered negligible—the addition of explicit solvent molecules can actually reduce the apparent charge transfer for PCET reactions to less than unity.[63] This may relate to a partial occupancy on H^+ while still in the double layer, and/or to delocalization errors in DFT.[5] Further discussion of computational models is deferred to the following section. In the present analysis, we have chosen to normalize the occupation of the projected H_{1s} state to its final value, such that both contributions scale with the reaction progress.

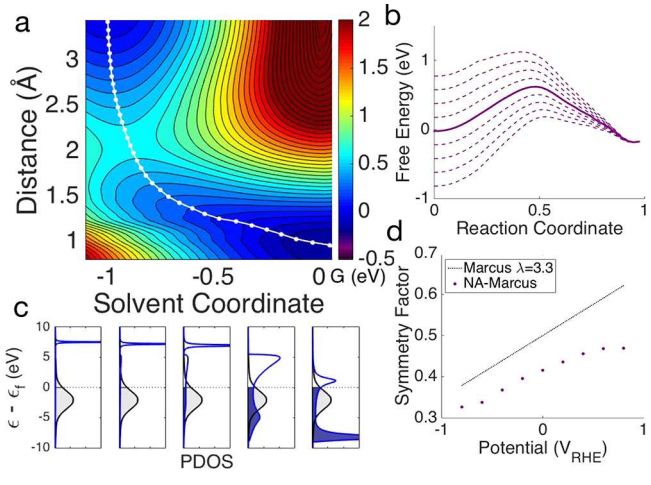

Figure 5. (a) Free energy surface computed for Volmer ($H^+ + e^- \leftrightarrow H^*$) reaction. (b) Minimum energy pathway at various overpotentials (solid line corresponds to the path traced in (a)). (c) Corresponding PDOS on H_{1s} orbitals (blue, *x*-axis zoomed and truncated for visibility of features) and scaled DOS for Pt (gray, Gaussian fit to d-band, flat sp-band). (d) ESFs determined from (b) compared with a standard Marcus model.

By computing a series of free energy surfaces (as in Figure 5a) with varying overpotential, we have estimated the symmetry factor as a function of potential. This is plotted in Figure 5d and compared to the basic Marcus theory with a reorganization energy of 3.3 eV (chosen to align the solvated proton energy to zero, but well within the approximation of eq 3). The ESFs are in qualitative agreement, but the computed values are uniformly smaller. One reason may be that the potential experienced by the proton as it approaches the surface is only weakly repulsive, whereas the force constant of the H-metal bond may give the product well of the free energy surface a sharper curvature. Asymmetric potentials are known to have the impact of shifting the symmetry factor line by approximately a constant.[64] Another cause for the departure from simple Marcus theory may be that the electrode-reactant separation distance corresponding to the transition state occurs systematically at further separations for larger negative overpotentials. Asymmetric potentials and distance dependences are addressable in the complete Marcus theory,[24] provided sufficient information on the relevant orbitals and vibrational modes is available. These factors implicitly manifest in Figure 5 as it is seeded with DFT energies at each separation distance.

The key point to take away from the above analysis is that the symmetry factor may differ non-negligibly from 1/2, even near equilibrium. The deviations may not be large enough to yield significant extrapolation errors over the small potential window typical of HER and HOR on Pt, but there may, however, be consequences in optimizing non-noble HER electrocatalysts. MoS_2, for example, is a promising material for the HER, and it has been shown that edge sites are primarily responsible for its activity.[65,66] These sites are calculated to have H-adsorption energies similar to Pt,[67] but they are quite scarce in comparison to basal plane sites. This scarcity leads to a requirement of significant overpotential, and therefore may imply that the optimal adsorption energy for H may not be precisely zero. More complex mechanisms, such as CO_2 reduction, with multiple bond breaking and formation steps, may have behavior that varies more widely.

DIRECT SIMULATIONS OF ELECTRON TRANSER

Finally, we call attention to recent developments in the explicit computation of electrochemical activation barriers. In some regards, there is a fine line between a "physically transparent" theory, such as that discussed above, and a simulation, which is still derived from a theory, but which begins to have too many interrelated parameters and too large a configuration space to give one immediate, generalizable insight. This trade-off underscores the need to establish highly accurate methods upon which to benchmark and validate more approximate models. Quantum chemical calculations have in principle the capability to approach chemical accuracy, although comprehensive models of the electrochemical interface, including solvent and electrolyte ion distributions, remain too computationally expensive to implement. As a starting point, numerous works have been directed toward characterizing the potential of the simulated electrode and the thermodynamics of the electrochemical interface. Estimates of reaction energies have been made accessible by the computational hydrogen electrode scheme,[5] which permits relation of a state with $H^+ + e^-$ to the computationally accessible energy of H_2 (and likewise for other

DOI: 10.1021/acscatal.7b03235
ACS Catal. 2017, 7, 8641−8652

redox pairs). However, explicit identification and control of potential within calculations remains challenging. Perhaps the most basic issue is that simulated systems are finite, and the transfer of an electron from electrode to reactant results in a change in potential. Periodic calculations, which are preferred for reactions on extended surfaces, must also be charge-neutral. Methods for controlling the potential of a periodic electrode surface have included direct addition of electrons with a homogeneous background counter-charge for neutrality,[68] distributing counter charge in a planar conductor[69] or throughout a continuous dielectric medium per the Poisson–Boltzmann equation,[70,71] and placing alkali or H atoms in an explicit water layer, such that charge moves to the surface and leaves ions in the water layer.[72] The atom-addition methods are somewhat more representative of real systems with electrolyte, but the control over potential is coarse—adding charge in integer increments creates large steps in potential unless the simulation cell is extremely large. Changes to the potential of a surface over the course of a full electron transfer reaction thus also tend to be large, regardless of the manner in which potential is established.

Several approaches have been taken to assigning a constant electrode potential over a simulated reaction path. Perhaps the most realistic (while still somewhat tractable) approach to date utilizes an iterative adjustment of injected charge to maintain constant potential, although it is still quite computationally costly.[7] Simple averaging between initial and final states has been suggested,[72] as has a cell-extrapolation scheme, whereby a process is modeled in increasingly sized unit cells and the reaction energy and change in work function are extrapolated to values converging at infinite size (negligible change in charge density).[4,73] Due to the high computational requirements of this method, a simpler charge-extrapolation method has been recently introduced, in which the interface is treated as an ideal capacitor.[5,74] Using a single barrier calculation and a charge allocation analysis (e.g., Bader), the charge transferred at transition and final states can be used to estimate the reaction energy and barrier fixed at the initial-state potential. The symmetry factor is identified as the charge transferred upon reaching the transition state. Uncertainties mainly stem from delocalization errors within DFT,[75] which can yield quantities of charge transfer that differ significantly from integer values. This may preclude accurate determination of the potential-dependence of the symmetry factor for some time.

In each of these methods solvation must still also be handled in an approximate way, either as continuum dielectric and/or with a few explicit water molecules (often an ice-like surface bilayer) with initial-state configurations representing reactants in the Helmholtz layer rather than beginning from bulk solvation. An alternative scheme has been developed in which potential-dependent barriers for electrochemical reactions are determined by extrapolating energetically equivalent non-electrochemical barriers—e.g. relating PCET to an equivalent H atom transfer.[11,36,76] In this method, the "equivalent" activation barrier is defined for the potential at which the atomic H species (adsorbed or bonded to water) would be in equilibrium with a solvated H^+ and e^- in the electrode. The barrier is then scaled with overpotential according to a Butler–Volmer symmetry factor, or more recently, a Marcus-type parabolic profile, fit to the points ascribed to initial, transition, and final states.[6] Definition of the reaction coordinate is still open to some interpretation and subject to uncertainties in solvent reorganization and charge allocation when, for example, extent of transfer is used as a coordinate. Although much progress has been made in the explicit calculation of electrochemical barriers, limitations related to finite system size including the representation of solvation, ion/field distribution, and maintenance of a constant potential still remain open problems with a need for further refinement. Delocalization error in particular may prove a significant challenge in moving beyond a linear (BV-type) model of the barriers.

COMPARISON OF APPROACHES

Having illustrated a number of models for electrochemical activation, we consider the impact that some of these treatments may have in identifying the "optimal" value of adsorption energy for the reaction sequence comprised of steps R1 + R2a above. Figure 6 shows the absolute value of rate computed for both positive and negative overpotentials using the (Gerischer)-Marcus model, eq 6. We compare cases with (a) equivalent reorganization energies for both steps ($\lambda_1 = \lambda_2 =$ 3 eV), and (b) values differing by 1 eV ($\lambda_1 = 4$ eV, $\lambda_2 = 3$ eV), which would correspond to just a 0.25 eV difference in intrinsic barrier. When the reorganization energies differ, it can be seen that the ideal adsorption energy exhibits a variation with potential, similar to what was shown in the BV analysis in Figure 2. The parameters of BV kinetics cannot be independently varied within Marcus theory due to their inherent relationships with the reorganization energy (eqs 4 and 5), but Figure 6b roughly corresponds to Figure 2c, with the addition of slowly varying symmetry factors.

To illustrate the possible implications of using fixed BV parameters to identify optimal catalysts over a large potential range, we compare, in Figure 7, volcano curves (vertical cuts through activity maps such as Figures 2 and 6) derived from BV and Marcus models. We make the approximation that Marcus-theory rate constants represent correct local values (i.e., at a given potential on a given material) for activation barriers and symmetry factors when fit with BV parameters. In other words, each BV activation barrier is given by a tangent plane to the local Marcus barrier, per eqs 2, 4, and 5. The volcano curves are shown at overpotentials of −0.3 V and −1.3 V for cases where the BV parameters are extracted locally at the operating potential, and where they are extrapolated from the equilibrium potential (each case being evaluated with the respective optimal adsorption energy for that potential). It can be seen in the figure that the BV result is in good agreement with the Marcus model when parameters are extracted near the chosen

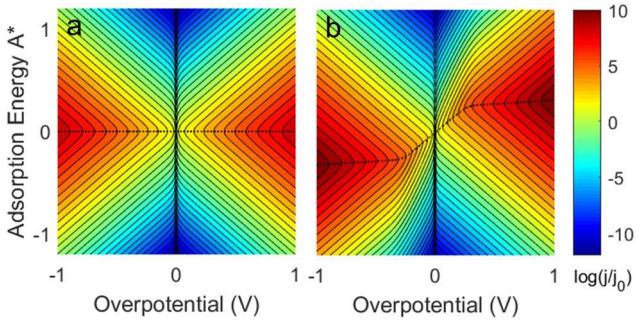

Figure 6. Activity maps (relative magnitude of rate) for forward and reverse two-step electrochemical reaction using Gerischer-Marcus model. (a): $\lambda_1 = \lambda_2 = 3$ eV and (b): $\lambda_1 = 4$ eV, $\lambda_2 = 3$ eV. The black dotted lines trace the maximum activity at each potential.

DOI: 10.1021/acscatal.7b03235
ACS Catal. 2017, 7, 8641−8652

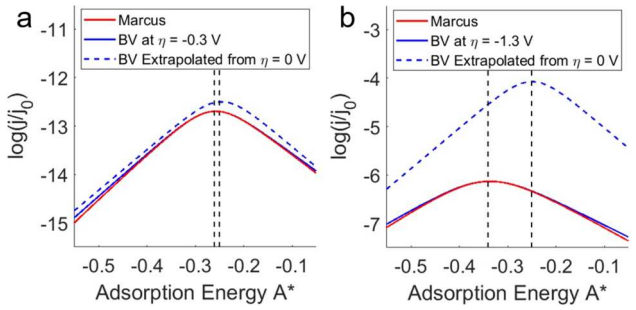

Figure 7. Volcano plots at −0.3 V (a) and −1.3 V (b) showing optimum adsorption energy found with Marcus theory and BV models. Both plots use BV parameters extrapolated from equilibrium, such that $\beta_1 = \beta_2 = 0.5$, $\Delta G^{\ddagger}_{0,1} = 1$, $\Delta G^{\ddagger}_{0,2} = 0.75$ eV, as well as local BV parameters at each potential determined via eqs 2, 4, and 5 with $\lambda_1 = 4$ eV, and $\lambda_2 = 3$ eV. Black vertical dotted lines indicate the peak of each curve.

operating potential. When extrapolated from 0 V, deviations arise. However, in this simple mechanism it appears that despite significant variation in the absolute values of rate constants, the shift in activity maximum requires a large overpotential to reach magnitudes of experimental consequence. At the −0.3 V condition, the volcano peak error shifts by a modest 0.01 eV. An additional volt of overpotential yields a 0.1 eV deviation, which is roughly the accuracy to which adsorption energy differences can be determined with DFT calculations.[77,78] As a point of reference, the symmetry factors at −1.3 V have moved from their equilibrium values of $\beta_1 = \beta_2 = 0.5$ to $\beta_1 = 0.30$ and $\beta_2 = 0.34$, while the apparent intrinsic barriers have shifted from $\Delta G^{\ddagger}_{0,1} = 1$, $\Delta G^{\ddagger}_{0,2} = 0.75$ to $\Delta G^{\ddagger}_{0,1} = 0.84$, $\Delta G^{\ddagger}_{0,2} = 0.67$ (all in eV). More complex mechanisms may have some potential to beget larger errors over smaller potential windows, but in general the conditions which generate significant shifts in symmetry factors (large overpotentials, large adsorption energies) will be most relevant when combatting elementary steps that have very large barriers (large reorganization energies). Since it is the ratio of reaction energy to reorganization energy that impacts the symmetry factor (see eq 5), extrapolation errors should only be expected to be significant when overpotentials are large relative to those where the rate is measured or where the barrier is calculated.

Finally, we point out that the particular example in Figure 7 does not represent a limiting magnitude of error, but rather just the differences that may arise between two simplistic models. As was shown in Figure 5d, it is possible that the true symmetry factors may deviate by larger amounts. We have excluded the NA-Marcus model from the present comparison because there is a significant configuration space (more degrees of freedom to map) for reaction R2a, and a proper NA model is also more involved than space permits. Nonetheless, that example serves to illustrate that actual parameter values have the potential to differ appreciably from BV or basic Marcus fits. A best practice in attempting to assess electrocatalyst kinetics would thus be to fit parameters as near to the neighborhood of typical operation on a given material as possible.

DISCUSSION AND OUTLOOK

Herein we have explored several models of electron transfer and discussed their respective impact on the identification of an optimal catalyst for a simple kinetic scheme. This study has illustrated the necessity to inform the design of catalytic materials with activation barrier estimates that are accurate at the intended operating potential of a reaction. We have also shown, however, that the approximation of constant elementary symmetry factors may often be adequate to assess the potential-dependencies of these barriers because activity maxima vary more substantially with (i) absolute differences in barriers and (ii) the (potential-dependent) reversibilities of the elementary steps. The impact of reversibilities is particularly important in electrocatalysis due to the operation of half-reactions near their individual equilibria—when a potential-determining elementary step is crossing the point of favorability, the optimal adsorption energy may still be a strong function of potential. In comparison, while the potential dependence of activation barriers can in principle play an important role, it is only the *differences* in such dependencies for multiple steps that contributes to changes in their respective degrees of rate control. Thus, from a practical perspective, shifts in predicted activity due to the assumption of constant ESFs will often not be large enough to alter the course of computational materials screening—usually any material within a few tenths of an eV to the optimum still merits testing. Reactions which require significant overpotentials and/or catalyst materials with large binding energies—factors that can induce large shifts in symmetry factor—will generally also involve commensurate reorganization energies, which have a dampening effect per eq 5.

Nonetheless, there are cases where a reaction may be performed at large overpotentials for reasons other than a large enthalpic barrier—for example, to overcome the low concentration of HER active sites on transition metal chalcogenides. Such instances may show significant deviations from symmetric BV kinetics across the potential span from equilibrium to high-current conditions. As illustrated with a Newns-Anderson-Marcus model for reductive H^+ adsorption, factors such as variability in the bond distance of the transition state and/or substantial differences between reactant and product force constants may yield a symmetry factor that deviates significantly from 1/2. While the value of ESFs in that model were generally smaller than 1/2, their potential-dependence was also still weak. Thus, a good compromise between accuracy and detail may be to utilize linear scaling models (BV-type kinetics) but to focus on obtaining good values for each of the constants at the most relevant conditions, rather than presuming symmetry factors of 1/2 and/or extrapolating barriers from the most convenient potential reference—frequently dictated by the equilibrium of a reference reaction or finite increments of potential set by simulation cell dimensions.[5,11] The fact that many real catalyst materials are also far from the theoretical optimum further enforces the need to evaluate barriers under relevant scenarios to determine how these materials should best be modified.

Chemical accuracy in the magnitude of activation barriers and symmetry factors will ideally be addressed with full quantum chemical calculations. The role of outer reorganization energy is large enough that these calculations will need to account for solvent interactions. While solvent contributions may be roughly constant in comparisons that are chemically analogous (e.g., the same reaction on different surfaces), the relative importance of sequential steps in complex mechanisms could be significantly impacted by differences in solvation. Explicit solvation is in principle ideal to capture specific coordination environments, but particular care must be taken with such models, as the initial-state solvent molecule

DOI: 10.1021/acscatal.7b03235
ACS Catal. 2017, 7, 8641−8652

placements are subject to bias. As computational power continues to grow, larger scale quantum molecular-dynamic simulations of the electrochemical interface will undoubtedly challenge previous assumptions and provide new insights. Calculations will also need to utilize transparent referencing schemes to establish constant reaction potentials and to utilize a well-benchmarked charge allocation scheme. The boundary for electrons shared by two centers can be defined in a number of ways, and more importantly, DFT is still subject to delocalization errors. Separation of charge transfer from hybridization will also require further consideration in defining symmetry factors according to, e.g., the partial charge transferred at the transition state.

More generally we have indicated that large multistep reactions should have the greatest likelihood of showing significant differences among relevant elementary step symmetry factors. It is to be expected from a microscopic picture of charge transfer that a strongly bound intermediate should have a low ESF for formation and a high ESF for removal. Scaling relations tend to dictate that sequences of elementary steps involving surface intermediates with correlated energies are apt to pass through both high and low energy intermediates—even on a good catalyst—and are thus apt to show a range of symmetry factors. At the same time, it may be recognized that the limiting cases of large energy change for a step coincide with the approaches to activationless or barrierless limits (quasi-equilibrium) of the step. Focus on the PDS and the thermodynamic overpotential may thus often be the first priority, but rates may have the potential to be further enhanced by lowering RDS barriers. Such an approach may also be limited by scaling relations, but these are not necessarily impossible to circumvent. Various approaches have been suggested to impart a differential stabilization to "related-but-different" surface moieties. These include the introduction of high-specificity surface ligands, alloying elements, or appropriate nanostructuring for geometric effects—though the promise of implementing these strategies at-will is often tempered by stability constraints. Manipulation of these variables is also contingent upon a certain level of knowledge about the active site and mechanism of reaction, and to this end there will be great needs in both simulation (particularly the role of solvent, adsorbed electrolyte species) and advanced experimental characterization (e.g., in situ spectroscopic probes). However, even simple experimental kinetic measurements, such as temperature dependence, concentration dependence, and isotopic labeling methods tend to be underutilized in electrocatalysis.

Finally, we acknowledge that the mechanistic insights put forth here are based on a hypothetical system and that the manifestations in real electrocatalytic processes may differ for any number of reasons. These may be simple, practical considerations such as the presence of mass transport limitations or stability issues such as restructuring or surface oxidation of a catalyst.[79] There may also be complexities that are inherent to the kinetics of a given reaction. Parallel pathways involving pure chemical steps are a simple example, though are straightforward to incorporate into modeling efforts. Another case could be the presence of rate-limiting outer-sphere electron transfer steps, which can undermine attempts to accelerate rates by tuning surface composition. This issue has been noted for the ORR in alkaline solution, which is found to involve an outer-sphere initiation step on many materials.[80] There may also be cases in which the thermodynamics and kinetics of crucial steps, either chemical or electrochemical, exhibit strong departures from the approximate shift given by the product of overpotential and charge transferred. These may arise through secondary influences such as the interaction between adsorbate dipoles and the electric field in the double layer. In a recent example, a comprehensive DFT model of the electrochemical interface (including solvent, electrolyte, and potential-dependence) was used to show that certain "pure-chemical" C−C coupling steps that may occur during CO_2 reduction over Cu may exhibit a rather strong potential dependence. It was found that the barrier for CO dimerization actually *increased* with applied (negative) overpotential, while a competing barrier for the reduction of CO to CHO decreased, consistent with experimental shifts in the selectivity profile.[7] Other studies of barriers for possible CO_2 reduction steps have shown that despite a higher thermodynamic driving force for CO to reduce to a CHO species, the barrier for reduction to COH is lower and governs selective conversion to methane over methanol.[36] Thus, we also note that while optimization of overall rate is always a worthy goal, selectivity must also often be prioritized and may be influenced by relatively subtle differences in the response of reaction energies and barriers toward potential. While such a long list of caveats certainly limits the reach of our concrete analysis, it also strengthens the underlying message. In such a complex environment as the electrochemical interface, accuracy cannot be guaranteed without a high degree of specificity, whether in simulation or experiment. Nonetheless, approximate models are necessary to generalize and guide priorities, both in experiment as well as in computationally intensive simulation. Care must simply be taken to ensure that these approximations do not cause omissions or a focus on a nonoptimal parameter space.

METHODS

Calculation Details. Plane-wave density functional theory calculations were performed using the Vienna Ab-Initio Simulation Package (VASP)[55,56] and the PBE exchange-correlation functional.[81] An energy cutoff of 450 eV was used in all calculations. The Brillouin zone integration was performed using a $(5 \times 5 \times 1)$ k-point Monkhorst−Pack grid[82] for initial surface relaxations and a $(17 \times 17 \times 1)$ k-point Monkhorst−Pack grid for DOS calculations. The surfaces were modeled by a (3×3) supercell with four metal layers and 16 Å of vacuum. Dipole corrections were used to avoid slab−slab interactions.[83] The first two layers were allowed to relax, while the bottom layers were fixed at the calculated nearest neighbor distance. The optimized surfaces (prerelaxed) in the absence of the hydrogen atom were used as input data to carry out the calculations to study the hydrogen desorption. For each Volmer reaction system, we performed a series of calculations for a single hydrogen atom adsorbed on a hollow site, and varied its separation from the surface. The prerelaxed surface was kept fixed while the H was allowed to relax in the xy-coordinates during these calculations. At each position, we calculated the adsorption energy and the DOS projected onto the 1s orbital of hydrogen. The calculations presented were performed without spin polarization.

AUTHOR INFORMATION

Corresponding Author

*E-mail: adam.holewinski@colorado.edu. Tel.: 1-303-492-3153.

DOI: 10.1021/acscatal.7b03235
ACS Catal. 2017, 7, 8641−8652

ORCID

Adam Holewinski: 0000-0001-8307-5881

Notes

The authors declare no competing financial interest.

■ ACKNOWLEDGMENTS

The authors acknowledge support from the National Science Foundation (CHE 1665176). A.R. also acknowledges support from the NSF Graduate Research Fellowship (#1144083). This work utilized the RMACC Summit supercomputer, which is supported by NSF awards ACI-1532235 and ACI-1532236, the University of Colorado Boulder, and Colorado State University. The Summit supercomputer is a joint effort of the University of Colorado Boulder and Colorado State University. The authors would also like to thank Prof. Hongliang Xin for helpful discussions.

■ REFERENCES

(1) Seh, Z. W.; Kibsgaard, J.; Dickens, C. F.; Chorkendorff, I.; Nørskov, J. K.; Jaramillo, T. F. *Science* **2017**, *355*, eaad4998.
(2) Jiao, Y.; Zheng, Y.; Jaroniec, M.; Qiao, S. Z. *Chem. Soc. Rev.* **2015**, *44*, 2060−2086.
(3) Kondratenko, E. V.; Mul, G.; Baltrusaitis, J.; Larrazábal, G. O.; Pérez-Ramírez, J. *Energy Environ. Sci.* **2013**, *6*, 3112−3135.
(4) Rossmeisl, J.; Skúlason, E.; Björketun, M. E.; Tripkovic, V.; Nørskov, J. K. *Chem. Phys. Lett.* **2008**, *466*, 68−71.
(5) Chan, K.; Nørskov, J. K. *J. Phys. Chem. Lett.* **2015**, *6*, 2663−2668.
(6) Akhade, S. A.; Bernstein, N. J.; Esopi, M. R.; Regula, M. J.; Janik, M. J. *Catal. Today* **2017**, *288*, 63−73.
(7) Goodpaster, J. D.; Bell, A. T.; Head-Gordon, M. *J. Phys. Chem. Lett.* **2016**, *7*, 1471−1477.
(8) Nørskov, J. K.; Rossmeisl, J.; Logadottir, A.; Lindqvist, L.; Kitchin, J. R.; Bligaard, T.; Jonsson, H. *J. Phys. Chem. B* **2004**, *108*, 17886−17892.
(9) Liu, X.; Xiao, J.; Peng, H.; Hong, X.; Chan, K.; Nørskov, J. K. *Nat. Commun.* **2017**, *8*, 15438.
(10) Chen, L. D.; Urushihara, M.; Chan, K.; Nørskov, J. K. *ACS Catal.* **2016**, *6*, 7133−7139.
(11) Rostamikia, G.; Mendoza, A. J.; Hickner, M. A.; Janik, M. J. *J. Power Sources* **2011**, *196*, 9228−9237.
(12) Hansen, H. A.; Viswanathan, V.; Nørskov, J. K. *J. Phys. Chem. C* **2014**, *118*, 6706−6718.
(13) Rhodes, C.; Hutchings, G. J.; Ward, A. M. *Catal. Today* **1995**, *23*, 43−58.
(14) Jacobsen, C. J. H.; Dahl, S.; Boisen, A.; Clausen, B. S.; Topsoe, H.; Logadottir, A.; Norskov, J. K. *J. Catal.* **2002**, *205*, 382−387.
(15) Boisen, A.; Dahl, S.; Nørskov, J. K.; Christensen, C. H. *J. Catal.* **2005**, *230*, 309−312.
(16) Koper, M. T. M. *J. Solid State Electrochem.* **2013**, *17*, 339−344.
(17) Sabatier, P. *Ber. Dtsch. Chem. Ges.* **1911**, *44*, 1984−2001.
(18) Bligaard, T.; Nørskov, J. K.; Dahl, S.; Matthiesen, J.; Christensen, C. H.; Sehested, J. *J. Catal.* **2004**, *224*, 206−217.
(19) Abild-Pedersen, F.; Greeley, J.; Studt, F.; Rossmeisl, J.; Munter, T. R.; Moses, P. G.; Skulason, E.; Bligaard, T.; Norskov, J. K. *Phys. Rev. Lett.* **2007**, *99*, 16105.
(20) Holewinski, A.; Xin, H.; Nikolla, E.; Linic, S. *Curr. Opin. Chem. Eng.* **2013**, *2*, 312−319.
(21) Bronsted, J. N. *Chem. Rev.* **1928**, *5*, 231−338.
(22) Evans, M. G.; Polanyi, M. *Trans. Faraday Soc.* **1938**, *34*, 11−24.
(23) Guidelli, R.; Compton, R. G.; Feliu, J. M.; Gileadi, E.; Lipkowski, J.; Schmickler, W.; Trasatti, S. *Pure Appl. Chem.* **2014**, *86*, 245−258.
(24) Marcus, R. A. *J. Chem. Phys.* **1965**, *43*, 679−701.
(25) *Electrochemical Methods: Fundamentals and Applications*, 2nd ed.; Bard, A. J., Faulkner, L. R., Eds.; John Wiley & Sons, Inc.: Hoboken, NJ, 2001.
(26) Henstridge, M. C.; Laborda, E.; Rees, N. V.; Compton, R. G. *Electrochim. Acta* **2012**, *84*, 12−20.
(27) Campbell, C. T. *Top. Catal.* **1994**, *1*, 353−366.
(28) Stegelmann, C.; Andreasen, A.; Campbell, C. T. *J. Am. Chem. Soc.* **2009**, *131*, 8077−8082.
(29) Campbell, C. T. *J. Catal.* **2001**, *204*, 520−524.
(30) Holewinski, A.; Linic, S. *J. Electrochem. Soc.* **2012**, *159*, H864−H870.
(31) Markovic, N. M.; Schmidt, T. J.; Stamenkovic, V. R.; Ross, P. N. *Fuel Cells* **2001**, *1*, 105−116.
(32) Keith, J. A.; Jacob, T. *Angew. Chem., Int. Ed.* **2010**, *49*, 9521−9525.
(33) Surendranath, Y.; Kanan, M. W.; Nocera, D. G. *J. Am. Chem. Soc.* **2010**, *132*, 16501−16509.
(34) Kucernak, A. R.; Zalitis, C. *J. Phys. Chem. C* **2016**, *120*, 10721−10745.
(35) Wang, J. X.; Springer, T. E.; Adzic, R. R. *J. Electrochem. Soc.* **2006**, *153*, A1732−A1740.
(36) Nie, X.; Esopi, M. R.; Janik, M. J.; Asthagiri, A. *Angew. Chem., Int. Ed.* **2013**, *52*, 2459−2462.
(37) Marcus, R. A. *J. Chem. Phys.* **1956**, *24*, 966−978.
(38) Hush, N. S. *J. Chem. Phys.* **1958**, *28*, 962−972.
(39) Marcus, R. A. *Discuss. Faraday Soc.* **1960**, *29*, 21−31.
(40) Levich, V. G. *Adv. Electrochem. Electrochem. Eng.* **1966**, *4*, 249−371.
(41) Dogonadze, R. R.; Kuznetsov, A. M. *Prog. Surf. Sci.* **1975**, *6*, 1−41.
(42) Cukier, R.; Nocera, D. *Annu. Rev. Phys. Chem.* **1998**, *49*, 337−369.
(43) Santos, E.; Schmickler, W. *Angew. Chem., Int. Ed.* **2007**, *46*, 8262−8265.
(44) Feaster, J. T.; Shi, C.; Cave, E. R.; Hatsukade, T.; Abram, D. N.; Kuhl, K. P.; Hahn, C.; Nørskov, J. K.; Jaramillo, T. F. *ACS Catal.* **2017**, *7*, 4822−4827.
(45) Mccrory, C. C. L.; Jung, S.; Peters, J. C.; Jaramillo, T. F. *J. Am. Chem. Soc.* **2013**, *135*, 16977−16987.
(46) Gerischer, H. *Advances in Electrochemistry and Electrochemical Engineering*; Wiley-VCH: Weinheim, 1961; Vol. *1*, pp 139−232.
(47) Hale, J. *J. Electroanal. Chem. Interfacial Electrochem.* **1968**, *19*, 315−318.
(48) Appleby, A. J.; Zagal, J. H. *J. Solid State Electrochem.* **2011**, *15*, 1811−1832.
(49) Schmickler, W. *J. Electroanal. Chem. Interfacial Electrochem.* **1986**, *204*, 31−43.
(50) Santos, E.; Lundin, A.; Pötting, K.; Quaino, P.; Schmickler, W. *Phys. Rev. B: Condens. Matter Mater. Phys.* **2009**, *79*, 1−10.
(51) Newns, D. M. *Phys. Rev.* **1969**, *178*, 1123−1135.
(52) Muscat, J. P.; Newns, D. M. *Prog. Surf. Sci.* **1978**, *9*, 1−43.
(53) Beyond ∼ 2.4 Å from the surface the H-atom begins to show spin polarization (in polarized calculations). This will cause some deviations to the computed free energy surface at high values of the solvent coordinate (upper right region of Figure 5a). However, the impact over the minimum energy path will be small because the occupancies go to zero at low *q* and high *d*.
(54) Nørskov, J. K. *Phys. Rev. B: Condens. Matter Mater. Phys.* **1982**, *26*, 2875−2885.
(55) Kresse, G.; Furthmüller, J. *Comput. Mater. Sci.* **1996**, *6*, 15−50.
(56) Kresse, G.; Furthmüller, J. *Phys. Rev. B: Condens. Matter Mater. Phys.* **1996**, *54*, 11169−11186.
(57) Nørskov, J. K. *Rep. Prog. Phys.* **1990**, *53*, 1253−1295.
(58) Lang, N. D.; Holloway, S.; Nørskov, J. K. *Surf. Sci.* **1985**, *150*, 24−38.
(59) Xin, H.; Linic, S. *J. Chem. Phys.* **2016**, *144*, 234704−234710.
(60) Shimanouchi, T. Molecular Vibrational Frequencies. In *NIST Chemistry WebBook, NIST Standard Reference Database Number 69*; Linstrom, P. J., Mallard, W. G., Eds.; National Institute of Standards and Technology: Gaithersburg, MD.
(61) Kandoi, S.; Gokhale, A. A.; Grabow, L. C.; Dumesic, J. A.; Mavrikakis, M. *Catal. Lett.* **2004**, *93*, 93−100.

DOI: 10.1021/acscatal.7b03235
ACS Catal. 2017, 7, 8641−8652

(62) Bader, R. F. W. *Chem. Rev.* **1991**, *91*, 893−928.
(63) Shi, C.; Chan, K.; Yoo, J. S.; Norskov, J. K. *Org. Process Res. Dev.* **2016**, *20*, 1424−1430.
(64) Laborda, E.; Henstridge, M. C.; Compton, R. G. *J. Electroanal. Chem.* **2012**, *667*, 48−53.
(65) Benck, J. D.; Hellstern, T. R.; Kibsgaard, J.; Chakthranont, P.; Jaramillo, T. F. *ACS Catal.* **2014**, *4*, 3957.
(66) Jaramillo, T. F.; Jorgensen, K. P.; Bonde, J.; Nielsen, J. H.; Horch, S.; Chorkendorff, I. *Science* **2007**, *317*, 100−102.
(67) Li, H.; Tsai, C.; Koh, A. L.; Cai, L.; Contryman, A. W.; Fragapane, A. H.; Zhao, J.; Han, H. S.; Manoharan, H. C.; Abild-Pedersen, F.; Nørskov, J. K.; Zheng, X. *Nat. Mater.* **2015**, *15*, 48−53.
(68) Filhol, J.-S. S.; Neurock, M. *Angew. Chem., Int. Ed.* **2006**, *45*, 402−406.
(69) Otani, M.; Sugino, O. *Phys. Rev. B: Condens. Matter Mater. Phys.* **2006**, *73*, 115407.
(70) Jinnouchi, R.; Anderson, A. B. *J. Phys. Chem. C* **2008**, *112*, 8747−8750.
(71) Rossmeisl, J.; Skúlason, E. M.; Björketun, M.; Tripkovic, V.; Nørskov, J. K. *Chem. Phys. Lett.* **2008**, *466*, 68−71.
(72) Skúlason, E.; Karlberg, G. S.; Rossmeisl, J.; Bligaard, T.; Greeley, J.; Jónsson, H.; Nørskov, J. K. *Phys. Chem. Chem. Phys.* **2007**, *9*, 3241−3250.
(73) Skulason, E.; Tripkovic, V.; Bjorketun, M. E.; Gudmundsdottir, S.; Karlberg, G.; Rossmeisl, J.; Bligaard, T.; Jonsson, H.; Norskov, J. K. *J. Phys. Chem. C* **2010**, *114*, 18182−18197.
(74) Chan, K.; Nørskov, J. K. *J. Phys. Chem. Lett.* **2016**, *7*, 1686−1690.
(75) Cohen, A. J.; Mori-Sánchez, P.; Yang, W. *Science* **2008**, *321*, 792−794.
(76) Nie, X.; Luo, W.; Janik, M. J.; Asthagiri, A. *J. Catal.* **2014**, *312*, 108−122.
(77) Medford, A. J.; Wellendorff, J.; Vojvodic, A.; Studt, F.; Abild-Pedersen, F.; Jacobsen, K. W.; Bligaard, T.; Nørskov, J. K. *Science* **2014**, *345*, 197−200.
(78) Hammer, B.; Hansen, L. B.; Norskov, J. K. *Phys. Rev. B: Condens. Matter Mater. Phys.* **1999**, *59*, 7413−7421.
(79) Engstfeld, A. K.; Brimaud, S.; Behm, R. J. *Angew. Chem., Int. Ed.* **2014**, *53*, 12936−12940.
(80) Ramaswamy, N.; Mukerjee, S. *J. Phys. Chem. C* **2011**, *115*, 18015−18026.
(81) Perdew, J. P.; Burke, K.; Ernzerhof, M. *Phys. Rev. Lett.* **1997**, *78*, 1396−1396.
(82) Monkhorst, H. J.; Pack, J. D. *Phys. Rev. B* **1976**, *13*, 5188−5192.
(83) Bengtsson, L. *Phys. Rev. B: Condens. Matter Mater. Phys.* **1999**, *59*, 12301−12304.

DOI: 10.1021/acscatal.7b03235
ACS Catal. 2017, 7, 8641−8652